CORA Cork Open Research Archive
Cartlann Taighde Oscailte Chorcaí

Title	Design of 3-legged XYZ compliant parallel manipulators with minimised parasitic rotations
Author(s)	Hao, Guangbo; Li, Haiyang
Publication date	2014-03
Original citation	Guangbo Hao and Haiyang Li. 2014. Design of 3-legged XYZ compliant parallel manipulators with minimised parasitic rotations . Robotica, available on CJO2014. doi:10.1017/S0263574714000575.
Type of publication	Article (peer-reviewed)
Link to publisher's version	http://journals.cambridge.org/action/displayJournal?jid=ROB http://dx.doi.org/10.1017/S0263574714000575 Access to the full text of the published version may require a subscription.
Rights	**Copyright © Cambridge University Press 2014. This article has been accepted for publication and will appear in a revised form, subsequent to peer review and/or editorial input by Cambridge University Press, in Robotica published by Cambridge University Press http://dx.doi.org/10.1017/S0263574714000575**
Item downloaded from	http://hdl.handle.net/10468/1515

University College Cork, Ireland
Coláiste na hOllscoile Corcaigh

Design of 3-Legged XYZ Compliant Parallel Manipulators with Minimised Parasitic Rotations

Guangbo Hao*, Haiyang Li
School of Engineering, University College Cork, Cork, Ireland
*Corresponding author, Email: g.hao@ucc.ie

ABSTRACT
This article deals with the design of 3-legged distributed-compliance XYZ compliant parallel manipulators (CPMs) with minimised parasitic rotations, based on the kinematically decoupled 3-PPPRR (P: prismatic joint, and R: revolute joint) and 3-PPPR translational parallel mechanisms (TPMs). The designs are firstly proposed using the kinematics substitution approach, with the help of the stiffness center (SC) overlapping based approach. This is done by appropriate embedded arrangement so that all of the SCs associated with the passive compliant modules overlap at the point where all of the input forces applied at the input stages intersect. Kinematostatic modelling and characteristic analysis are then carried out for the proposed large-range 3-PPPRR XYZ CPM with overlapping SCs. The results from finite element analysis (FEA) are compared to the characteristics found for the developed analytical models, as are experimental testing results (primary motion) from the prototyped 3-PPPRR XYZ CPM with overlapping SCs. Finally, issues on large-range motion and dynamics of such designs are discussed, as are possible improvements of the actuated compliant P joint. It is shown that the potential merits of the designs presented here include a) minimised parasitic rotations by only using three identical compliant legs; b) compact configuration and small size due to the use of embedded design; c) approximately kinematostatically decoupled design capable of easy control; and d) monolithic fabrication for each leg using existing planar manufacturing technologies such as electric discharge machining (EDM).

KEYWORDS: *Translational parallel manipulators*; *Compliant mechanisms*; *Parasitic rotations*; *Overlapping stiffness centers*; *Distributed compliance; 3-legged configuration*

1. Introduction

Compliant parallel manipulators (CPMs) are flexure mechanisms that transfer loads or displacements by the deformation of their compliant members, and belong to a class of parallel-type manipulators. CPMs benefit from eliminated backlash and friction, no need for lubrication, reduced wear and noise, monolithic configuration, etc [1]. There are increasing needs for high-precision (up to nano-positioning) manipulators such as XYZ CPMs. An XYZ CPM is generally composed of a fixed base and a motion stage, interconnected by compliant members. The motion stage is capable of translating along the X-, Y-, and Z-axes actuated by three actuators indirectly. XYZ CPMs have been used in many emerging applications such as atomic force microscopes/scanning tunnelling microscopes (AFMs/STMs), nano-positioning stages, bio-cell injectors, adjusting mountings, and precision optical alignment devices [2-8].

In the design of CPMs for high-precision manipulators, good performance characteristics have been specified along with the nanometric motion quality (<10nm) in terms of motion repeatability, accuracy (i.e. lack of error), and

resolution (i.e. minimum incremental motion). These good characteristics [9-10] include: 1) large range of motion along the desired direction (also large-range motion along the intending degree of freedom), 2) inherently well-constrained parasitic error motion (also the minimal undesired motion along the degree of constraint), 3) minimal cross-axis coupling motion [1] (also kinematostatic decoupling/output-decoupling that is the minimal undesired motion along non-intending degree of freedom), 4) maximal actuator isolation (also input-decoupling that is the minimal transverse motion of the actuator), 5) minimal lost motion (also the minimal displacement difference between the actuator and the motion stage), 6) maximal drive stiffness (also the maximal overall stiffness between the point of actuation and the motion stage), 7) low thermal and manufacturing sensitivities, 8) compactness of the configuration, 9) minimal number of geometrical parameters (for example using identical modules), 10) low cost, and 11) desired dynamic performance (including high natural frequency and no uncontrollable mass).

It should be noted that large range of motion is the most desirable but a challenging issue in designing compliant mechanisms, which is generally affected by the following factors: a) system size (or beam length), b) beam thickness, c) material selection (depending on ratio of Yield Strength to Young's Modulus), d) linear actuator, and e) conceptual-level configuration design. Improving the last factor is the most effective way to raise the motion range by using the distributed-compliance joints and/or multi-level (serial) embedded arrangement without considering the material and actuators since the increase of the beam length can make the configuration bulky, and the decrease of the beam thickness may result in the significant decrease of stiffness and other issues such as manufacturability. In addition, the number of non-controllable motion masses should be reduced from the good dynamics point of view.

In 3-legged XYZ compliant manipulators with distributed compliance for large range of motion, undesired parasitic rotation inherently accompanies its primary translation, adversely affecting the positioning/scanning accuracy unless suitable measures are taken. For example, a commonly-used parallelogram flexure mechanism produces a transverse primary motion caused by the force acting at the tip of the flexure mechanism with the consequence that active rotation compensation is needed to maintain a zero rotation at the tip. This issue on the negative parasitic rotation is one of the shortcomings of the well-known compact serial XYZ flexure

---

[1]There are two classes of decoupling: one is the kinematic decoupling, and the other is the kinematostatic decoupling. Kinematic decoupling can be further classified into two types: complete decoupling and partial decoupling. We only concern the complete kinematic decoupling, which refers to that each independent output motion is controlled by only one input motion. Kinematostatic decoupling means that one primary output translational displacement is only affected by the actuation force along the same direction, which describes the relationship between the input force and output motion. This decoupling (not absolute) is also called the output-decoupling/minimal cross-axis coupling in CPMs. Kinematostatic coupling may lead to complicated motion control, which is the sufficient condition of kinematic decoupling.

stage by Martock Design [8]. A 6-legged, fully-symmetrical, arrangement fails to better constrain the parasitic rotation for the decoupled XYZ CPMs with distributed compliance. This is because the fully-symmetrical arrangement is more complex and much bulkier, and contains an auxiliary leg in the vertical direction (usually the Z-axis), which leaves less space for the motion stage.

There are plenty of typical designs of XYZ compliant manipulators from non-commercial academic inventions [11-15] and commercialised products in market [16-17]. Despite their many good characteristics, these existing designs can still be improved. The designs in [11, 12] produce a small range of motion and large stress concentration and are very sensitive to manufacturing, due to the use of lumped-compliance modules. Recently, Awtar et al [13] proposed a novel large-range XYZ parallel kinematic flexure mechanism with geometrically decoupled DOF (degree of freedom) using identical flexure plates/leaves, which has a more compact and simpler construction. However, this design also suffers from the effect of parasitic rotations, and has relatively low out-of-plane stiffness and large lost motion (both due to the out-of-plane bending of the flexure leaves thereof). In particular, its three actuation directions are skewed and cannot intersect at the center of the multi-axis motion stage so that its applications are limited to the low-payload and/or low-speed mode. A hybrid-motion CPM (partially CPM) combining macro-motion (driven by DC motor) and micro-motion (driven by PZT actuator) was developed in [14] in order to achieve large range of motion and high resolution. However, this hybrid motion CPM is kinematostatically coupled and bulky, and has poor motion repeatability and large stress concentration. Hao and Kong [15] reported a decoupled XYZ CPM composed of identical spatial compliant modules, which, however, still has the issues on negative parasitic rotations and challenging fabrication. Meanwhile, several commercialised products in the market from leading companies such as Thorlabs [16] and Physikinstrumente (PI) [17] are subject to their own limitations such as serial configuration, no strategy for well constraining parasitic motion, and/or small range of motion.

The object of this paper, therefore, is to propose novel 3-legged XYZ CPMs that overcome the shortcomings described above with particular emphasis on minimising the parasitic rotations. This paper is organised as follows. Section 2 proposes the stiffness center (SC) overlapping based approach. In Sec. 3, two types of kinematostatically decoupled 3-legged XYZ CPMs are presented based on the kinematically decoupled 3-PPPRR (P: prismatic joint, and R: revolute joint) and 3-PPPR translational parallel mechanisms (TPMs) with the use of the approach proposed in Sec. 2. Kinematostatic

modelling and characteristic analysis are implemented in Secs. 4 and 5, respectively. Analytical results are compared with those obtained from finite element analysis (FEA) in Sec. 6, with primary motion verified by experiment in Sec. 7. Large range of motion, dynamics, and improvements of the actuated compliant P joint are further discussed in Sec. 8, before final conclusions are drawn.

2. SC Overlapping Based Approach

It is known [18] that increasing the spanning size or decreasing the beam's in-plane thickness of a parallelogram flexure mechanism can slightly alleviate the parasitic rotation that accompanies a primary translation produced by the force acting at the mechanism's tip. However, these approaches inevitably result in a bulky configuration, or one that is difficult to fabricate and has a dramatically decreased primary stiffness. Additionally, the primary translation coupling with the spanning parameter nonlinearly contributes to the parasitic rotation effect and reduces the parasitic rotation stiffness [18].

A partial SC based design was discussed in [9] for a 2-PP XY CPM, which can only minimise the parasitic rotational yaw well if only *one* actuation force is applied. The SC refers to a point through which an actuation force along the primary motion direction is applied on the motion stage of a planar-motion/spatial-motion compliant module to produce the primary translation with minimised parasitic rotation. The SC is independent of the changes of spanning size and the beam's thickness. The indicated SC of an example parallelogram flexure module is the symmetric center of all compliant beams as clearly demonstrated in Fig. 1, which can be determined by the following nonlinear parasitic rotation equation [18]:

$$\theta_{sz} = \frac{1}{2(W/L)^2}[\frac{1}{d} + (Y_s/L)^2 r]\{\frac{M}{EUT^3/(12L)}$$
$$-\frac{F_y/[EUT^3/(12L^2)]}{2a+Pe/[EUT^3/(12L^2)]}[2c+\frac{Ph}{EUT^3/(12L^2)}]\} \quad (1)$$

where W, T, U and L are the mechanism's half spanning size, the beam's in-plane thickness, and the beam's out-of-plane thickness, and the beam's length, respectively. The non-dimensional characteristic numbers for a beam are: a=12, c=−6, d=12/(T/L)^2, e=1.2, i=−0.6, r=1/700, and h=−0.1. P (tensile force along the X-axis), F (transverse force along the Y-axis) and M (moment about the Z-axis) are all the loads acting at the center of the motion stage's bottom-plane. As indicated in Eq. (1), the parasitic rotation is zero if M=−FL/2 and P=0. Without loss of generality, we can conclude that as long as P is relatively small and M=−FL/2, the parasitic rotation can be regarded as zero.

(a) Undeformed configuration

(b) Deformed configuration for applied force acting at the stiffness center

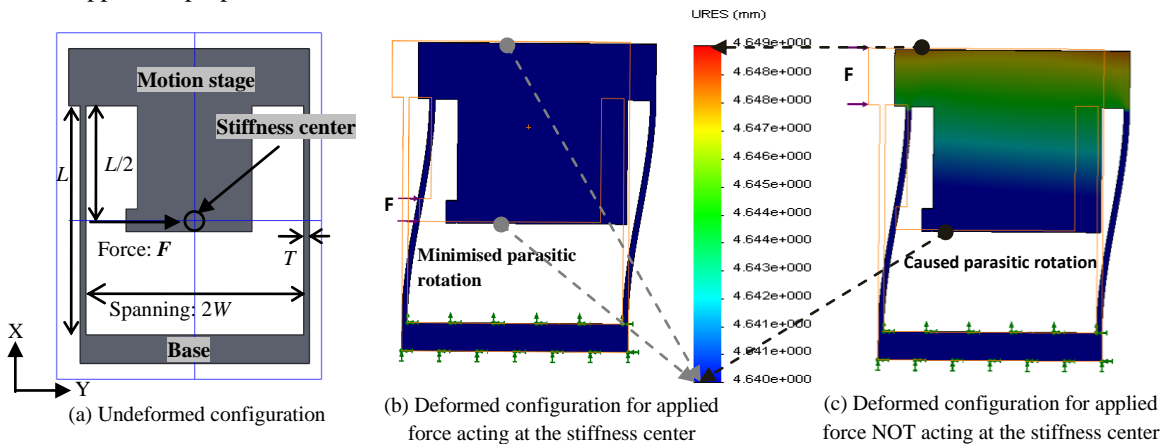(c) Deformed configuration for applied force NOT acting at the stiffness center

Fig. 1 SC demonstration for a parallelogram module

2

In order to better reduce the parasitic rotations of multi-DOF translational CPMs, a full SC overlapping based approach can be conceived. Such an approach rearranges the passive compliant modules connected to the motion stage in the translational CPMs, so that all of the SCs associated with the passive compliant modules overlap at the point where all of the applied input forces intersect. The design examples obtained from this approach are shown in the next section.

3. Design of 3-legged Distributed-Compliance XYZ CPMs with Minimised Parasitic Rotations

A novel 3-legged XYZ CPM with minimised parasitic rotations can be proposed, based on a proper configuration of rigid-body TPMs (via kinematics substitution), such that the SCs of the passive compliant modules overlap as described in Sec. 2. This section will focus on the conceptual design of a variety of 3-legged XYZ CPMs with minimised parasitic rotations.
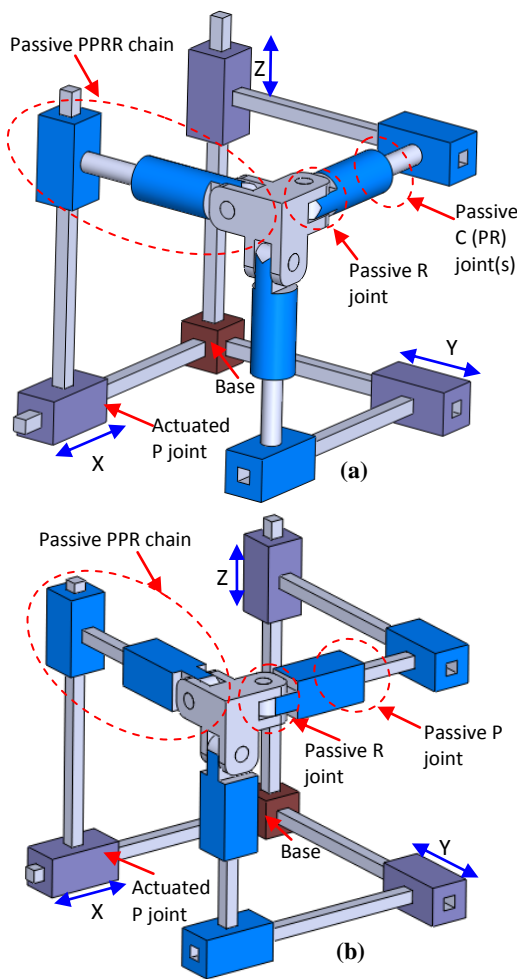

Fig. 2 A kinematically decoupled 3-PPPRR TPM (a) and a kinematically decoupled 3-PPPR TPM (b)

The works on 3-DOF TPMs [19] may provide a basis to construct novel XYZ CPMs. Figure 2 shows two types of kinematically decoupled 3-legged 3-DOF TPMs, an exactly-constrained 3-PPPRR TPM and an over-constrained 3-PPPR TPM, suitable for our needs. In both cases, the P joint connected to the base is the actuated joint, and the PPRR/PPR joint directly connected to the motion stage is the passive joint. Note that all of the R joints are inactive [19] due to the inherent constraint of the XYZ TPMs, and the three motion planes associated with the three passive PP kinematic chains in the three legs are orthogonal to produce

the kinematic decoupling. Each actuated P joint is arranged to be perpendicular to the passive PP motion plane in each leg so that the configuration of the resulting 3-DOF TPMs can be used to construct the following kinematostatically decoupled XYZ CPMs.

A large-range XYZ CPM with overlapping SCs (Fig. 3) can be obtained by the following two steps.

a) Replace the actuated P joint and the passive PPRR chain in each leg of the 3-PPPRR TPM (Fig. 2(a)) with a well-behaving actuated compliant P joint (*two double parallelogram flexure modules, composed of leaf beams, in mirror symmetry*) and a passive compliant PPRR joint (*a compliant two-beam module composed of two parallel wire beams*), respectively.

b) Make all of the SCs associated with the three passive compliant PPRR joints overlap at the point where all of the input forces applied at the input stages intersect, by appropriate embedded arrangement.

The geometrical parameter definitions will be shown in Secs. 4 and 5. More details about the large range of motion can be referred to Sec. 8.1.
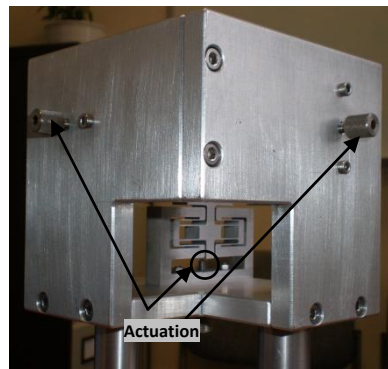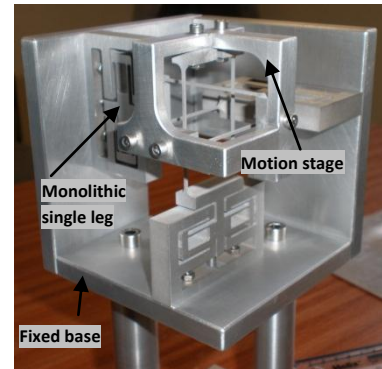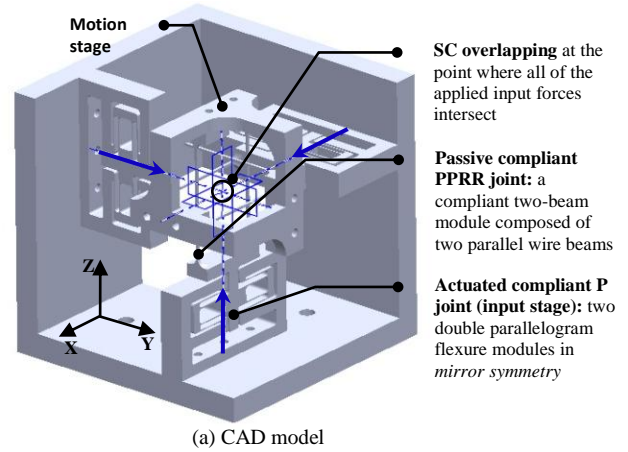

(a) CAD model

(b) Prototype: view 1

(c) Prototype: view 2

Fig. 3 Large-range 3-PPPRR XYZ CPM with overlapping SCs

3

The compliant two-beam module used in the large-range XYZ CPM proposed in Fig. 3 contains the inherent cross-axis coupling. Although this cross-axis coupling is very small and easily addressed in motion systems via feedback controls, an improved large-range XYZ CPM with reduced cross-axis coupling and overlapping SCs can be obtained by replacing each passive compliant two-beam module in Fig. 3 with a better-behaving compliant *double* two-beam module, as shown in Fig. 4. This compliant double two-beam module is similar to the arrangement in the double parallelogram flexure module.

Moreover, an XYZ CPM with high stiffness (and therefore good dynamics) can be obtained as shown in Fig. 5. It uses a multi-beam strategy (i.e. elasticity average) in all of the compliant joints, and adopts the two mirror-symmetrical *basic* parallelogram flexure modules as the actuated compliant P joint without a non-controllable mass. The details of what constitutes good dynamics will be discussed further in Sec. 8.2.
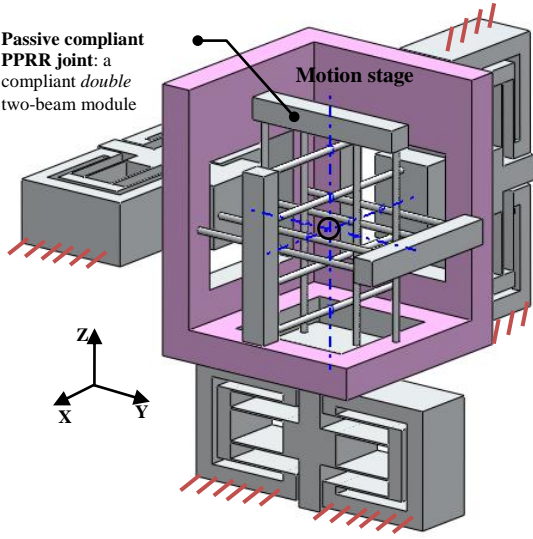

Fig. 4 Improved large-range 3-PPPRR XYZ CPM with reduced cross-axis coupling and overlapping SCs
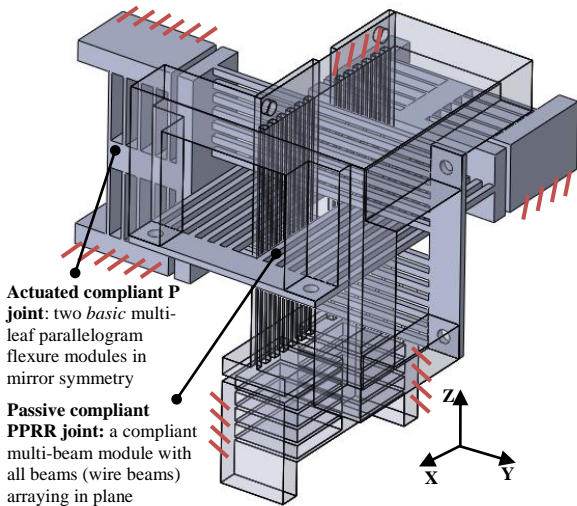

Fig. 5 High-stiffness/high-frequency 3-PPPRR XYZ CPM with overlapping SCs

Using a similar procedure to the above, another type of large-range XYZ CPM with overlapping SCs (Fig. 6) can be generated based on the 3-PPPR TPM (Fig. 2(b)). Here, the actuated P joint in each leg of the 3-PPPR TPM is replaced with the same actuated compliant P joint as used in Figs. 3 and 4, and the passive compliant PPR chain is replaced with a passive compliant PPR joint (a compliant four-beam module composed of four parallel wire beams for planar motion). All of the SCs associated with the three passive compliant PPR joints are then made to overlap at the point where all of the applied input forces intersect.
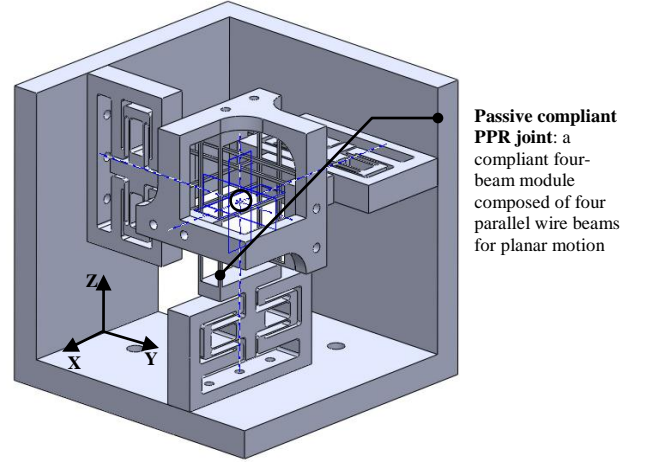

Fig. 6 Large-range 3-PPPR XYZ CPM

4. Kinematostatic Modelling of the 3-PPPRR XYZ CPM with overlapping SCs

4.1 Linear modelling

In this section, all of the modelling assume Euler-Bernoulli beams with small deformations, and the material's non-linearity is ignored. As an example, the 3-PPPRR XYZ CPM with overlapping SCs (Fig. 3) is selected for analytical modelling based on the linear modelling method [15]. Similar to Ref. [15], the normalization-based strategy is adopted here to represent loads and displacements in order to simplify the representations and derivations, which means that all translational displacements and length parameters are normalized by the actual length L of the symmetrical cross-section beam in the passive compliant two-beam module, forces are normalized by EI/L^2, and moments are normalized by EI/L. The lower-case letters are used to refer to the corresponding normalized variables/parameters. Here, E denotes the Young's modulus, and I represents the second moment of the cross-sectional area of the same symmetrical wire beam.

Since the 3-PPPRR XYZ CPM (Fig. 3) is composed of three identical legs, we can focus on deriving the stiffness and compliance matrices of Leg 1 that produces the X-axis actuation. The stiffness and compliance matrices for Legs 2 and 3 can be obtained by applying the appropriate coordinate transformations to the results found for Leg 1.

For a passive compliant two-beam module with loads and displacements defined at the center of the bottom-plane of its own motion stage, with the normalized spanning parameter of $2w$, we obtain its stiffness matrix as follows:

$$\mathbf{K}_{\mathrm{pm}} = \sum_{i=1}^{2} \mathbf{D}_i^{\mathrm{T}} \mathbf{K} \mathbf{D}_i \qquad (2)$$

where

$$\mathbf{D}_i = \begin{bmatrix} 1 & 0 & 0 & 0 & z_i' & -y_i' \\ 0 & 1 & 0 & -z_i' & 0 & x_i' \\ 0 & 0 & 1 & y_i' & -x_i' & 0 \\ 0 & 0 & 0 & 1 & 0 & 0 \\ 0 & 0 & 0 & 0 & 1 & 0 \\ 0 & 0 & 0 & 0 & 0 & 1 \end{bmatrix},$$

and

$$\mathbf{K} = \begin{bmatrix} d & 0 & 0 & 0 & 0 & 0 \\ 0 & 12 & 0 & 0 & 0 & -6 \\ 0 & 0 & 12 & 0 & 6 & 0 \\ 0 & 0 & 0 & 1/(1+v) & 0 & 0 \\ 0 & 0 & 6 & 0 & 4 & 0 \\ 0 & -6 & 0 & 0 & 0 & 4 \end{bmatrix}.$$

The variables in $\mathbf{D}_i$ are defined as follows: $x_1'=0$, $y_1'=w$, and $z_1'=0$; $x_2'=0$, $y_2'=-w$, and $z_2'=0$. In $\mathbf{K}$, $d=12/(T/L)^2$ for the square cross-section beam with an actual thickness of T, and v is the Poisson's ratio of the material.

Thus, the compliance matrix of the passive compliant two-beam module can be derived from Eq. (2) as follows, assuming that the associated loads and displacements are both specified at its SC that is the symmetrical center of the two beams.

$$\mathbf{C}_{sc} = \mathbf{J}_{pm}\mathbf{K}_{pm}^{-1}\mathbf{J}_{pm}^{T} \tag{3}$$

where

$$\mathbf{J}_{pm} = \begin{bmatrix} 1 & 0 & 0 & 0 & 0 & 0 \\ 0 & 1 & 0 & 0 & 0 & -0.5 \\ 0 & 0 & 1 & 0 & 0.5 & 0 \\ 0 & 0 & 0 & 1 & 0 & 0 \\ 0 & 0 & 0 & 0 & 1 & 0 \\ 0 & 0 & 0 & 0 & 0 & 1 \end{bmatrix},$$

which is a transformation matrix obtained from $\mathbf{D}_i$ in Eq. (2).

Because the primary translational stiffness of the passive compliant two-beam module is negligible compared to the off-axis stiffness of the actuated compliant P joint, the actuated compliant P joint in Leg 1 has the following simplified compliance matrix:

$$\mathbf{C}_a = \begin{bmatrix} c_a, & \mathbf{0}_{1\times5} \\ \mathbf{0}_{5\times1}, & \mathbf{0}_{5\times5} \end{bmatrix}_{6\times6} \tag{4}$$

where c_a represents the normalized primary compliance of the actuated compliant P joint, and $\mathbf{0}_{5\times5}$ represents a 5×5 zero matrix representing infinitely large off-axis stiffness.

Based on Eqs. (3) and (4), the stiffness matrix of Leg 1 for the loads and displacements defined at the same SC point of all of the three passive two-beam modules is

$$\mathbf{K}_{\text{leg}1} = (\mathbf{C}_a + \mathbf{C}_{sc})^{-1}. \tag{5}$$

Using Eq. (5), the stiffness matrix of the XYZ CPM for the loads and displacements defined at the overlapping SCs on the motion stage can be derived as

$$\mathbf{K}_{\text{cpm}1} = \mathbf{K}_{\text{leg}1} + \mathbf{R}_{\text{leg}2}\mathbf{K}_{\text{leg}1}\mathbf{R}_{\text{leg}2}^{-1} + \mathbf{R}_{\text{leg}3}\mathbf{K}_{\text{leg}1}\mathbf{R}_{\text{leg}3}^{-1} \tag{6}$$

where

$$\mathbf{R}_{\text{leg}2} = \begin{bmatrix} \cos(\pi/2) & -\sin(\pi/2) & 0 & 0 & 0 & 0 \\ \sin(\pi/2) & \cos(\pi/2) & 0 & 0 & 0 & 0 \\ 0 & 0 & 1 & 0 & 0 & 0 \\ 0 & 0 & 0 & \cos(\pi/2) & -\sin(\pi/2) & 0 \\ 0 & 0 & 0 & \sin(\pi/2) & \cos(\pi/2) & 0 \\ 0 & 0 & 0 & 0 & 0 & 1 \end{bmatrix},$$

$$\times \begin{bmatrix} 1 & 0 & 0 & 0 & 0 & 0 \\ 0 & \cos(\pi/2) & -\sin(\pi/2) & 0 & 0 & 0 \\ 0 & \sin(\pi/2) & \cos(\pi/2) & 0 & 0 & 0 \\ 0 & 0 & 0 & 1 & 0 & 0 \\ 0 & 0 & 0 & 0 & \cos(\pi/2) & -\sin(\pi/2) \\ 0 & 0 & 0 & 0 & \sin(\pi/2) & \cos(\pi/2) \end{bmatrix}$$

and

$$\mathbf{R}_{\text{leg}3} = \begin{bmatrix} \cos(-\pi/2) & 0 & \sin(-\pi/2) & 0 & 0 & 0 \\ 0 & 1 & 0 & 0 & 0 & 0 \\ -\sin(-\pi/2) & 0 & \cos(-\pi/2) & 0 & 0 & 0 \\ 0 & 0 & 0 & \cos(-\pi/2) & 0 & \sin(-\pi/2) \\ 0 & 0 & 0 & 0 & 1 & 0 \\ 0 & 0 & 0 & -\sin(-\pi/2) & 0 & \cos(-\pi/2) \end{bmatrix}.$$

$$\times \begin{bmatrix} 1 & 0 & 0 & 0 & 0 & 0 \\ 0 & \cos(-\pi/2) & -\sin(-\pi/2) & 0 & 0 & 0 \\ 0 & \sin(-\pi/2) & \cos(-\pi/2) & 0 & 0 & 0 \\ 0 & 0 & 0 & 1 & 0 & 0 \\ 0 & 0 & 0 & 0 & \cos(-\pi/2) & -\sin(-\pi/2) \\ 0 & 0 & 0 & 0 & \sin(-\pi/2) & \cos(-\pi/2) \end{bmatrix}$$

Accordingly, the compliance matrix, $\mathbf{C}_{\text{cpm}1}$, and the load-displacement relationships for the XYZ CPM are obtained as

$$\mathbf{C}_{\text{cpm}1} = \mathbf{K}_{\text{cpm}1}^{-1}, \tag{7a}$$

$$\mathbf{X}_s = \mathbf{C}_{\text{cpm}1}\mathbf{F} \tag{7b}$$

where

$\mathbf{F} = [f_x, f_y, f_z, m_x, m_y, m_z]^T$ and $\mathbf{X}_s = [x_s, y_s, z_s, \theta_{sx}, \theta_{sy}, \theta_{sz}]^T$, which are the loads and displacements of the motion stage, respectively. f_x, f_y and f_z are the normalized forces along the X-, Y- and Z-axes, respectively, and m_x, m_y and m_z are the normalized moments about the X-, Y- and Z-axes, respectively. x_s, y_s and z_s are the normalized translational displacements along the X-, Y- and Z-axes, respectively, and θ_{sx}, θ_{sy} and θ_{sz} are the rotational displacements about the X-, Y- and Z-axes, respectively.

It should be noted that the lost translational motion between the motion stage and the input stage (the actuated P joint) is negligibly small, which means that each actuation force along each axis acting at the same SC point on the motion stage can be equivalent to that acting at the actuated compliant P joint. This is attributed to that, in the 3-legged configuration, the lost motion in one leg only contributes to the low-stiffness translation of the passive compliant modules in the other two legs. Therefore, in the subsequent modelling and analysis, f_x, f_y and f_z are regarded as the normalized actuation forces imposed on the input stages along the X-, Y- and Z-axes, respectively.

4.2 Nonlinear modification

According to the above analytical compliance matrix (Eq. (7)) and the proposed nonlinear modification method in [20], simple but relatively accurate nonlinear load-displacement equations can be written to capture the slight cross-axis coupling effect due to the parasitic translation of passive compliant modules as

$$\begin{cases} x_s = f_x\mathbf{C}_{\text{cpm}1}(1,1) - 0.6(f_y\mathbf{C}_{\text{cpm}1}(2,2))^2 \left(\dfrac{\mathbf{C}_{\text{cpm}1}(2,2)}{c_a}\right) \\ \quad - 0.6(f_z\mathbf{C}_{\text{cpm}1}(3,3))^2 \left(\dfrac{\mathbf{C}_{\text{cpm}1}(3,3)}{c_a}\right) \\ y_s = f_y\mathbf{C}_{\text{cpm}1}(2,2) - 0.6(f_x\mathbf{C}_{\text{cpm}1}(1,1))^2 \left(\dfrac{\mathbf{C}_{\text{cpm}1}(1,1)}{c_a}\right) \\ \quad - 0.6(f_z\mathbf{C}_{\text{cpm}1}(3,3))^2 \left(\dfrac{\mathbf{C}_{\text{cpm}1}(3,3)}{c_a}\right) \\ z_s = f_z\mathbf{C}_{\text{cpm}1}(3,3) - 0.6(f_x\mathbf{C}_{\text{cpm}1}(1,1))^2 \left(\dfrac{\mathbf{C}_{\text{cpm}1}(1,1)}{c_a}\right) \\ \quad - 0.6(f_y\mathbf{C}_{\text{cpm}1}(2,2))^2 \left(\dfrac{\mathbf{C}_{\text{cpm}1}(2,2)}{c_a}\right) \end{cases} \tag{8a}$$

$$\begin{cases} x_{\mathrm{ax}} = f_x C_{\mathrm{cpm1}}(1,1) + 0.6(f_y C_{\mathrm{cpm1}}(2,2))^2(1 - \dfrac{C_{\mathrm{cpm1}}(2,2)}{c_a}) \\[2mm] \quad + 0.6(f_z C_{\mathrm{cpm1}}(3,3))^2(1 - \dfrac{C_{\mathrm{cpm1}}(3,3)}{c_a}) \\[2mm] y_{\mathrm{ay}} = f_y C_{\mathrm{cpm1}}(2,2) + 0.6(f_x C_{\mathrm{cpm1}}(1,1))^2(1 - \dfrac{C_{\mathrm{cpm1}}(1,1)}{c_a}) \\[2mm] \quad + 0.6(f_z C_{\mathrm{cpm1}}(3,3))^2(1 - \dfrac{C_{\mathrm{cpm1}}(3,3)}{c_a}) \\[2mm] z_{\mathrm{az}} = f_z C_{\mathrm{cpm1}}(3,3) + 0.6(f_x C_{\mathrm{cpm1}}(1,1))^2(1 - \dfrac{C_{\mathrm{cpm1}}(1,1)}{c_a}) \\[2mm] \quad + 0.6(f_y C_{\mathrm{cpm1}}(2,2))^2(1 - \dfrac{C_{\mathrm{cpm1}}(2,2)}{c_a}) \end{cases} \quad (8b)$$

where the symbols: x_{ax}, y_{ay} and z_{az} are the normalized primary translational displacements of the three input stages (actuated compliant P joints) along the X-, Y- and Z-axes, respectively. $C_{\mathrm{cpm1}}(i,j)$ denotes the element in the i-row and the j-column in $\mathbf{C}_{\mathrm{cpm1}}$ (Eq. (7a)), and $C_{\mathrm{cpm1}}(1,1) = C_{\mathrm{cpm1}}(2,2) = C_{\mathrm{cpm1}}(3,3)$. The high-order terms on the right-hand side of each equation are due to the nonlinear kinematic effect upon the beam's axis displacement in the passive compliant joint.

4.3 Linear modelling of a 3-PPPRR XYZ CPM without overlapping SCs

The modelling process for a corresponding 3-PPPRR XYZ CPM without overlapping SCs is similar to the process mentioned above (refer to the example in Fig. A.1). Therefore, the following will only show the differences in the model derivation.

With the loads and displacements defined at the center of the cubic motion stage of the XYZ CPM, the compliance matrix of the passive compliant two-beam module is obtained as

$$\mathbf{C}_{\mathrm{mc}} = \mathbf{J}_{\mathrm{pml}} \mathbf{K}_{\mathrm{pm}}^{-1} \mathbf{J}_{\mathrm{pml}}^{\mathrm{T}} \qquad (9)$$

where

$$\mathbf{J}_{\mathrm{pml}} = \begin{bmatrix} 1 & 0 & 0 & 0 & 0 & 0 \\ 0 & 1 & 0 & 0 & 0 & w \\ 0 & 0 & 1 & 0 & -w & 0 \\ 0 & 0 & 0 & 1 & 0 & 0 \\ 0 & 0 & 0 & 0 & 1 & 0 \\ 0 & 0 & 0 & 0 & 0 & 1 \end{bmatrix},$$

of which w is half of the side length of the motion stage in a cubic form, also the half spanning size of the passive compliant two-beam module.

In terms of Eq. (9), the stiffness matrix of Leg 1 with the loads and displacements defined at the center of the motion stage needs to be re-written as

$$\mathbf{K}_{\mathrm{leg1}} = (\mathbf{C}_a + \mathbf{C}_{\mathrm{mc}})^{-1}. \qquad (10)$$

Therefore, the compliance matrix, $\mathbf{C}_{\mathrm{cpm2}}$, of the XYZ CPM without using the SC overlapping based strategy can be obtained by substituting Eq. (10) into Eq. (6) to deal with the loads and displacements specified at the center of the motion stage.

5. Characteristic Analysis

The parameters chosen for the XYZ CPM with overlapping SCs (Fig. 3) are as follows: L=50 mm (actual length of the wire beam), T=1 mm (actual in-plane thickness of the wire beam), and W=15 mm (actual half spanning size of the compliant two-beam module); L_1=12.5 mm (actual length of the leaf), U_1=10 mm (actual out-of-plane thickness of the leaf) and T_1=0.5 mm (actual in-plane thickness of the leaf); v=0.33 (Poisson's Ratio) and E=69 GPa (Young's Modulus) for a standard alluminum alloy AL6061-T651.

The corresponding normalized values are obtained: w=15/50=0.3, d=12/(1/50)^2=30000, and

$$c_a = (\frac{1^4}{12 \times 50^3}) / (\frac{24 \times 10 \times 0.5^3}{12 \times 12.5^3}) = 5.21 \times 10^{-4}.$$

Substituting the above values into Eq. (7), we have

$$\mathbf{C}_{\mathrm{cpm1}} = 10^{-4} \times \begin{bmatrix} 5.2398 & 0 & 0 & 0 & 0 & 0 \\ 0 & 5.2398 & 0 & 0 & 0 & 0 \\ 0 & 0 & 5.2398 & 0 & 0 & 0 \\ 0 & 0 & 0 & 1.8492 & 0 & 0 \\ 0 & 0 & 0 & 0 & 1.8492 & 0 \\ 0 & 0 & 0 & 0 & 0 & 1.8492 \end{bmatrix}. \qquad (11)$$

where $C_{\mathrm{cpm1}}(1,1)$, $C_{\mathrm{cpm1}}(2,2)$ or $C_{\mathrm{cpm1}}(3,3)$ is nearly equal to c_a, which reflects that the primary translation stiffness of the actuated P joint is much larger than that of the passive compliant two-beam module. Therefore, the assumption of Eq. (4) is reasonable since the off-axis stiffness of the actuated P joint is much larger than its primary translational stiffness.

Equation (11) shows a diagonal compliance matrix. This implies that the 3-PPPRR XYZ CPM with overlapping SCs (Fig. 3) is *kinematostatically decoupled*, and has *zero parasitic motion* under the action of only actuation forces. It is noted that the actuation forces produce no rotations irrespective of the decrease of the spanning size or the increase of the beam's thickness.

Similarly, substituting the same parameters into $\mathbf{C}_{\mathrm{cpm2}}$ yields

$$\mathbf{C}_{\mathrm{cpm2}} = 10^{-4} \times \begin{bmatrix} 5.2402 & -0.0002 & -0.0002 & 0 & 0.0185 & -0.0185 \\ -0.0002 & 5.2402 & -0.0002 & -0.0185 & 0 & 0.0185 \\ -0.0002 & -0.0002 & 5.2402 & 0.0185 & -0.0185 & 0 \\ 0 & -0.0185 & 0.0185 & 1.8389 & -0.0001 & -0.0001 \\ 0.0185 & 0 & -0.0185 & -0.0001 & 1.8389 & -0.0001 \\ -0.0185 & 0.0185 & 0 & -0.0001 & -0.0001 & 1.8389 \end{bmatrix}. \qquad (12)$$

Equation (12) indicates that the 3-PPPRR XYZ CPM without overlapping SCs (Fig. A.1) is not completely kinematostatically decoupled, and has *inherent parasitic rotations* under the action of only actuation forces because the left corner 3×3 sub-matrix is not a zero matrix. It can be shown that the same actuation forces produce about 8.5 times larger rotations if w reduces from 0.3 to 0.1, and generates about 3 times larger rotations if d decreases from 30000 to 10000.

Both Eqs. (11) and (12) suggest that the applied actuation force cannot generate any rotation about itself.

It deserves mentioning that the conclusions that the actuation forces result in *zero parasitic motion* in the linear model in Eq. (11) is slightly inaccurate, for two reasons:

a) the modelling for Eq. (11) is based on the assumptions that the off-axis stiffness of the actuated P joint is infinitely large, and that some parts are absolutely rigid;

b) the zero parasitic rotation is only valid for the single-axis loading and instantaneous motion (i.e. linear model), and cannot reflect the nonlinear cases within the whole motion space.

Therefore, the small physical parasitic rotaions still exist. However, because the primary translational stiffness of the passive compliant two-beam module is negligible compared

to the off-axis stiffness of the actuated compliant P joint, and because the internal tensile force on the passive compliant two-beam module is small enough, the proposed SC overlapping based method reduces the parasitic rotations to a very small level over the motion range. In the next section, the analytical results for the parasitic rotations are still assumed to be zero, based on Eq. (11), for simplification.

The actual primary translational stiffness of the 3-PPPRR XYZ CPM with overlapping SCs can be further calculated based on Eq. (11) as

$$K_T = \frac{69000 \times 1^4}{5.2398 \times 10^{-4} \times 12 \times 50^3} = 87.79 \text{N/mm}. \quad (13)$$

The motion range of the prototyped XYZ CPM with overlapping SCs is controlled by the minimal value of the following two equations:

$$\Delta_{\text{leaf}} = \frac{2}{3\eta} \frac{\sigma_s}{E} \frac{L_1^2}{T_1^2} = \frac{2}{3\eta} \times 4 \times 10^{-3} \times \frac{12.5^2}{0.5}, \quad (14)$$

$$\Delta_{\text{wire-beam}} = \frac{1}{6\eta} \frac{\sigma_s}{E} \frac{L^2}{T} = \frac{1}{6\eta} \times 4 \times 10^{-3} \times \frac{50^2}{1}. \quad (15)$$

It can be seen that the motion range of the system is determined by Eq. (14). Using a safety factor of $\eta = 1.11$ the uni-directional motion range is equal to 0.75 mm (i.e. a total bi-directional motion range of 1.5 mm).

6. FEA Comparisons

In this section, nonlinear FEA static elastic deformation results are obtained to compare with the analytical results obtained in Sec. 5 (Eq. 11) for the 3-PPPRR XYZ CPM with overlapping SCs (Fig. 3). Single-axis loading is conducted via FEA to analyse the primary stiffness and the parasitic rotations, which is then used to verify how effectively the SC overlapping based strategy works. Here, commercial software, Comsol, is selected to carry out the FEA using tetrahedral elements and the finest meshing option available with others default.

The translation in the Y-direction caused by only the actuation force along the same axis is shown in Fig. 7. The nominal primary stiffness difference between the FEA result and the analytical result (Eq. (11) or Eq. (13)) is about 2.63% when the analytical result as the denominator.
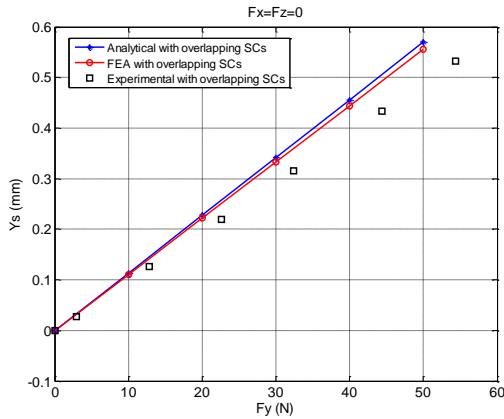

Fig. 7 Primary motion in the Y-direction

The parasitic rotation comparisons are illustrated in Figs. 8-10. FEA results show that the parasitic rotation absolute value about the X-axis is less than 1.0×10^{-5} rad and that about the Z-axis is less than 6.33×10^{-5} rad over the primary motion of about 1.5 mm in the bi-direction, while the parasitic rotation about the actuation force direction is much smaller with the magnitude lower than 8.3×10^{-7} rad. Note

that Figs. 8-9 clearly validate that the 3-PPPRR XYZ CPM with overlapping SCs (Fig. 3) significantly reduces the parasitic rotations compared with the 3-PPPRR XYZ CPM without overlapping SCs (Fig. A.1).
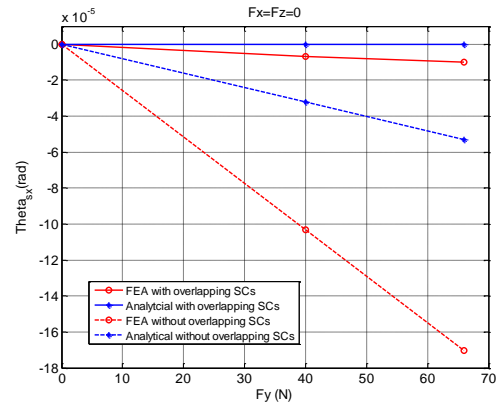
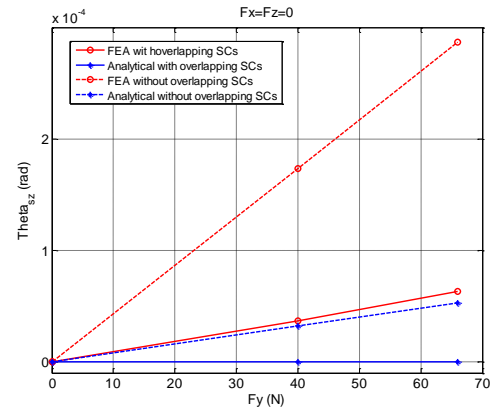

Fig. 8 Parasitic rotation about the X-axis

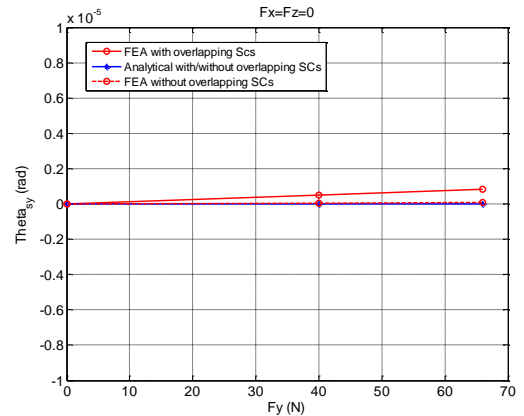**Fig. 9 Parasitic rotation about the Z-axis**

Fig. 10 Parasitic rotation about the Y-axis

Multi-axis loading is also studied to capture the cross-axis coupling effects. As shown in Fig. 11, the nonlinear model (Eq. 8a) has a very good agreement with the FEA model with a small difference of about 2.55%.

The modal shapes of the 3-PPPRR XYZ CPM with overlapping SCs obtained from the FEA results are shown in Fig. 12 with natural frequencies larger than 180 Hz.

The difference between the analytical results and the FEA results shown above are acceptable for most applications, which may stem from inaccuracy of either the analytical modelling or the meshing method and solver ability of FEA. The relatively large difference in parasitic rotations can probably be attributed to the fact that the off-axis stiffness of the actuated P joint is assumed to be infinitely large, and some parts are also assumed to be absolutely rigid in the modelling. Therefore, it is envisaged that the increase of out-

of-plane thickness of the actuated compliant P joint (i.e. increasing the off-axis stiffness), or the enhancement of rigidity of the motion stage can further reduce the effect of parasitic rotations. In addtion, the rotational angle magnitudes in two directions (about X and Z-axes) for single-axis loading under F_y differ due to the fact that the actuated compliant P joint has different in-plane and out-of-plane off-axis rotational stiffnesses.
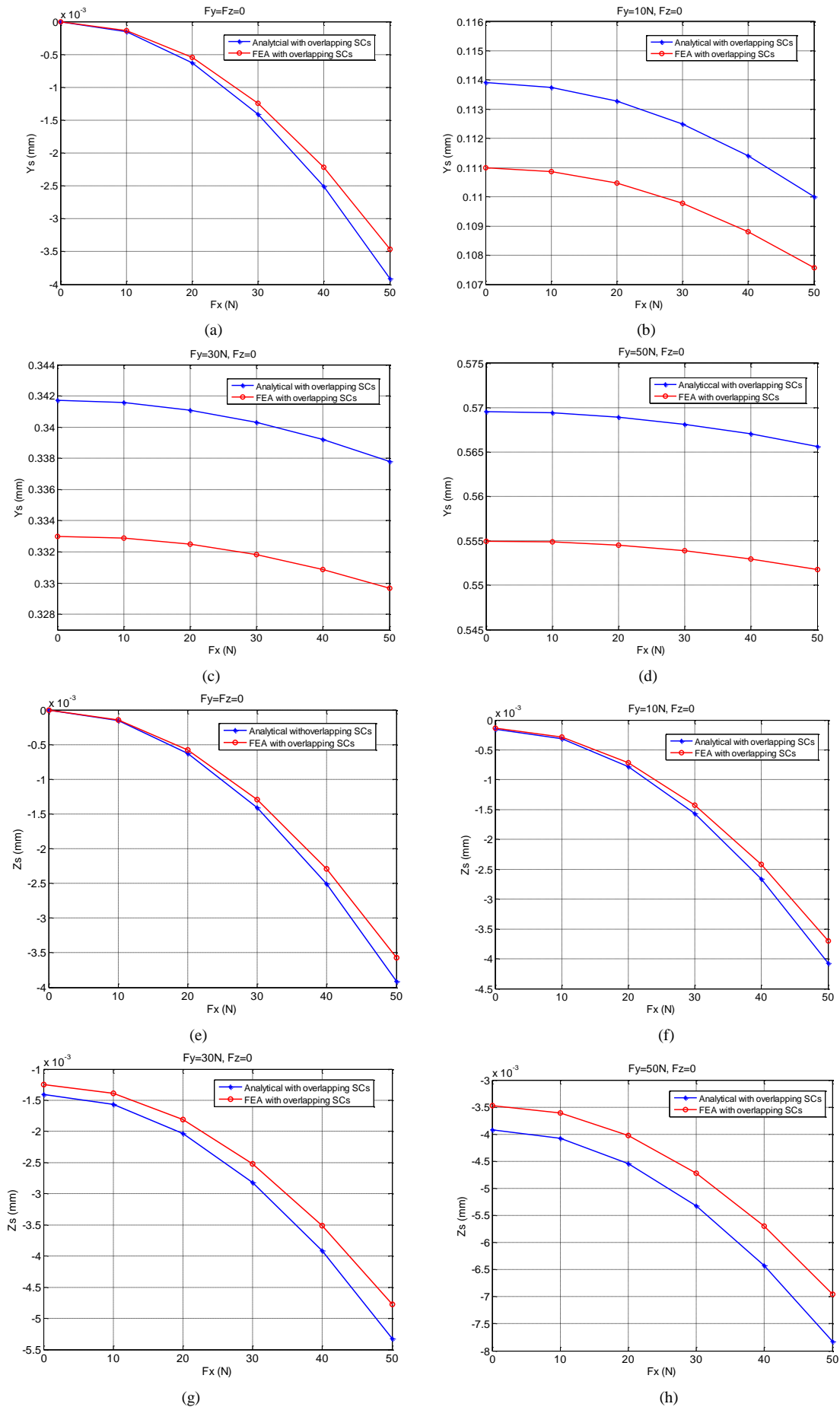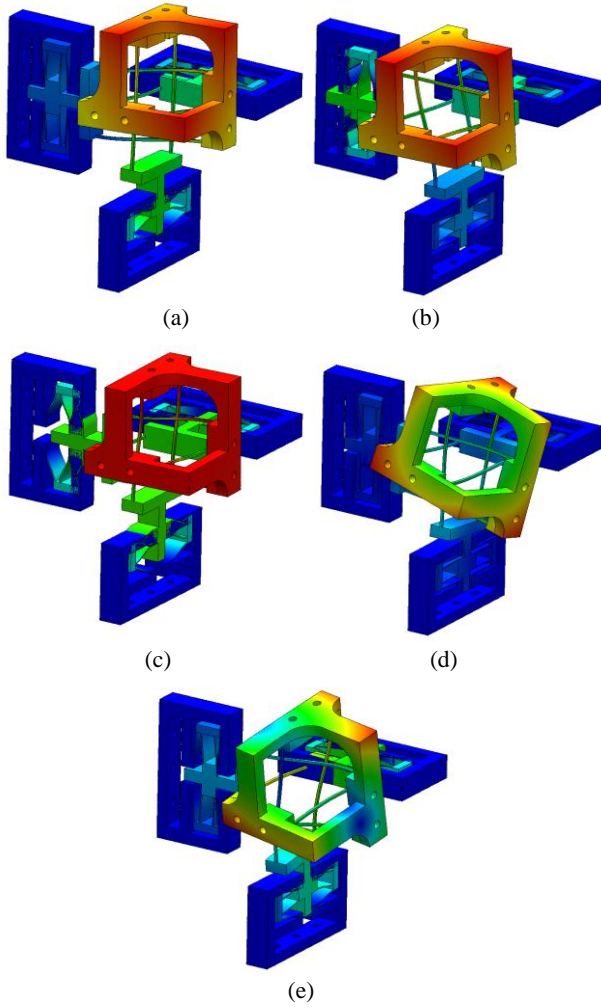

Fig. 11 Cross-axis coupling effect

8

Fig. 12 Modal shapes from FEA: (a) modal shape 1 (182.7Hz); (b) modal shape 2 (182.75Hz); (c) modal shape 3 (202.18Hz); (d) modal shape 4 (379.86Hz); (e) modal shape 5 (482.1Hz)

The analytical model proposed in this paper is very useful because it enables rapid analysis and design synthesis compared to the time-consuming FEA.

7. Prototyping and Testing

The 3-PPPRR XYZ CPM with a peripheral dimension of 105mm×105mm×105mm and bi-directional motion range of 1.5 mm along each axis, made of the standard aluminium alloy AL6061-T651, has been prototyped (Figs. 3(b) and 3(c)) by using the EDM and CNC milling machining. Here, each compliant leg is monolithically fabricated by EDM.

The experimental rig shown in Fig. 13 is for testing the primary motion along each axis (X- or Y- axis). Two-axis pushing loading is applied using inverted loading weights guided by two linear bearings with pulleys. The displacements along the two loading axes are then measured by two low-force digital indicators with a motion resolution of 0.001mm and a spring force of 0.4-0.7N (Digimatic Indicators, Mitutoyo Corporation, Japan).

The tested primary motion along the Y-axis is shown in Fig. 7. As predicted, the experimental results are lower than the analytical/FEA results, which may mainly be induced by the manufacturing fillet at the end of the beam. It merits mentioning that assembly and manufacturing error also plays a role on the system performance characteristics.

Due to the experimental condition limitations (displacement sensor resolution, etc), the tiny parasitic rotation and the very small cross-axis coupling effect cannot be appropriately captured in this paper.
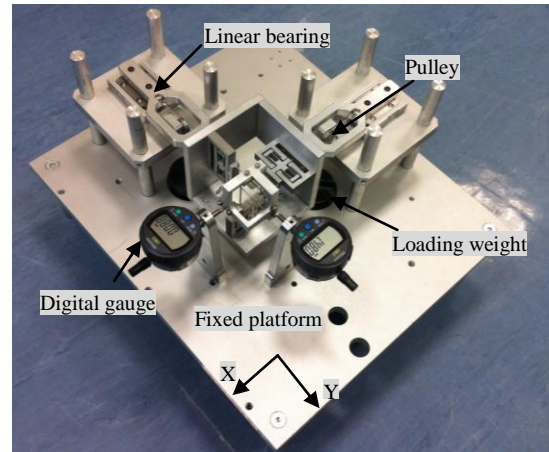

Fig. 13 Testing rig

8. Discussions

8.1. Large-range-of-motion considerations

The present XYZ CPM shown in Fig. 3 can generate millimetre-level large range of motion at a conceptual level (not just changing the thickness and length of beams) since it uses the *distributed compliance* in all the compliant joints and adopts two mirror-symmetrical *double* parallelogram modules as the actuated compliant P joint. Note that mirror-symmetry here is a parallel configuration, which is always adopted for better actuator isolation.

Each double parallelogram module used in the actuated compliant P joint is in a multi-level (serial) embedded arrangement that plays an important role in largely alleviating the load-stiffening effect and the parasitic translation. If two mirror-symmetrical *basic* (single-level) parallelogram modules are used as the actuated compliant P joint, the resulting motion stage cannot generate large-range motion. The reasons fall into two aspects: a) a very large internal tensile force is caused to compensate for the inherent large parasitic translation of the basic parallelogram module in the mirror-symmetrical compliant P joint, which significantly increases the tensile stress causing yield under large range of motion; b) the above produced internal tensile force makes a great contribution to produce much larger load-stiffening effect that significantly nonlinearly increases the primary motion stiffness over motion resulting in the use only small-motion and large-force linear actuators such as PZT actuators.

The employed distributed compliance can not only produce large-range motion, but also result in relatively small primary stiffness to promote the use of large-range voice coil actuators since a larger primary stiffness will require a bulkier voice coil actuator to produce higher peak force. In addition, the distributed-compliance based design can tolerate the manufacturing error and reduce the stress-concentration effect.

8.2 Dynamics considerations

From the well-known dynamic equation, it is clear that it is possible to reduce the mass or increase the stiffness to raise the modal frequencies for improving the dynamic performance of the proposed XYZ CPMs. Therefore, one can further increase the beam number (i.e. using multi-beam

strategy as shown in Fig. 5) to raise the primary stiffness (and therefore the first natural frequency) without affecting the maximal motion range. In addition to the above method, one may also improve the dynamic performance by using a high-order controller to achieve a high bandwidth greater than the first natural frequency [10].

It should be noted that the double parallelogram module used in the actuated compliant P joint has an under-constrained/non-controllable secondary stage/mass with one translational DOF, meaning that the secondary stage can still move even though we have its motion stage and base fixed. Therefore, the present large-range XYZ CPM (Fig. 3) can behave well under quasi-static/low-speed motion mode, in which the secondary stages involved in the actuated double parallelogram modules do not vibrate uncontrollably. However, to run the large-range XYZ CPM at an appreciable speed, a trade-off has to be made between good characteristics, such as large range of motion achieved through the use of the double parallelogram modules involving the secondary stages, and the uncontrollable vibration mentioned above. Therefore, from the good dynamics point of view, the number of non-controllable motion masses should be reduced as much as possible, which suggests that the multi-level (serial) embedded arrangement (with non-controllable motion mass) should not be adopted for each passive compliant joint in each leg. This suggestion will bring a small cross-axis coupling effect that can be easily addressed in motion systems via feedback controls.

Furthermore, the under-constrained secondary stages involved in the compliant joints must be avoided in the high-frequency XYZ CPM so that two basic multi-leaf parallelogram modules in mirror symmetry are used as the actuated compliant P joint in Fig. 5.

Because the high-frequency design requires high stiffness and a larger primary stiffness requires a bulkier voice coil actuator to produce higher peak force, as a result of the high-frequency nanopositioning, the PZT actuator has to be used to produce large force but relatively small motion range. Therefore, there is always a trade-off between high frequency and large-range motion in high-precision motion systems.

8.3 Improvements of the actuated compliant P joint

In order to achieve large-range motion without under-constraint in the XYZ CPM, some improvements can be employed. The first strategy is to add a slaving mechanism (i.e. lever mechanism) to connect the motion stage and secondary stage of the double parallelogram module so that a 2:1 motion ratio is achieved [21]. The second strategy is to adopt a new exactly-constrained design to replace the double parallelogram module in the XYZ CPM. One example replacement is a novel parallelogram flexure mechanism composed of four identical monolithic cross-spring flexural pivots [22], where via sophisticated design the parasitic translation of the parallelogram mechanism can be compensated by the rotational centre shifts of the cross-spring flexural pivots thereof. Therefore, the load-stiffening effect is also largely eliminated in the two mirror-symmetrical novel parallelogram flexure mechanisms as the actuated compliant P joint [22]. However, both improvements will increase the design complexity and make the actuated compliant P joint bulkier.

9. Conclusions

3-legged XYZ CPMs with minimised parasitic rotations have been proposed using a kinematics substitution approach combined with the SC overlapping based method. Designs for large range of motion and high-stiffness/high-frequency requirements have been illustrated and discussed. Also, kinematostatic modelling has been implemented with comparisons with the FEA results and/or experimental results.

The designs proposed in this paper have the following main potential characteristics:

- *Minimised parasitic rotations* (zero instantaneous parasitic rotations) by only using three *identical* compliant legs;
- *Compact configuration* and *small size* due to the use of embedded design;
- *Approximately kinematostatic decoupling* capable of easy control; and
- *Monolithic fabrication* for each leg using existing manufacturing technologies such as EDM.

In addition, the design solutions developed in this paper have negligible lost motion and good actuator isolation characteristics, and don't have any issues with the locking mechanism and additional servicing costs compared to any one existing flexure based solution in market.

Nonlinear modelling, optimisation and more accurate experimental testing deserve future investigation.

References

1. Howell, L.L., 2001, *Compliant Mechanisms*, Wiley, New York.
2. Schitter, G., Thurner, P.J, and et al, 2008, "Design and Input-Shaping Control of a Novel Scanner for High-Speed Atomic Force Microscopy", *Mechatronics*, Vol. 18:282-288.
3. Werner, C., Rosielle, P.C.J.N., Steinbuch, M., 2010"Design of a Long Stroke Translation Stage for AFM", *International Journal Machine Toolsand Manufacture*, Vol. 50(2):183-190.
4. Weckenmann, A., and Hoffmann, J., 2007, "Long Range 3D Scanning Tunnelling Microscopy", *CIRP Annals - Manufacturing Technology*, Vol. 56(1):525–528.
5. Shinno, H., Yoshioka, H., 2010, "A Newly Developed Three-Dimensional Profile Scanner with Nanometer Spatial Resolution", *CIRP Annals – Manufacturing Technology*, Vol. 59(1):525–528.
6. Gorman, J. J., and Dagalakis, N. G., 2003, "Force Control of Linear Motor Stages for Microassembly," *ASME International Mechanical Engineering Conference and Exposition*, November 15–21, 2003, Washington, DC, USA.
7. Vettiger, P., Despont, M., Drechsler, U., Durig, U., Haberle, W., Lutwyche, M. I., Rothuizen, H. E., Stutz, R., Widmer, R., and Binnig, G. K., 2000, "The Millipede—More Than One Thousand Tips for Future

AFM Data Storage", *IBM Journal of Research and Development*, Vol. 44(3): 323-340.

8. Martock Design Limited, 1987, *Adjustable Mountings*, United States Patent, No.:4635887.

9. Awtar, S., and Slocum, A. H., 2007, "Constraint-Based Design of Parallel Kinematic XY Flexure Mechanisms", *Journal of Mechanical Design*, Vol. 129(8):816-830.

10. Awtar, S., and Parmar, G., 2010, "Design and a Large Range XY Nanopostioning System", *Proceedings of the ASME 2010 International Design Engineering Technical Conferences & Computers and Information in Engineering Conference*, August 15–18, 2010, Montreal, Quebec, Canada. DETC2010-28185

11. Li, Y., Xu, Q., 2011, "A Totally Decoupled Piezo-Driven XYZ Flexure Parallel Micropositioning Stage for Micro/Nanomanipulation", *IEEE Transactions on Automation Science and Engineering*. Vol. 8(2):265–279.

12. Yue, Y., Gao, F., Zhao, X., and Ge, Q., 2010, "Relationship among Input-Force, Payload, Stiffness and Displacement of a 3-DOF Perpendicular Parallel Micro-Manipulator", *Mechanism and Machine Theory*, Vol.45 (5):756–771.

13. Awtar, S., and Ustick, J., and Sen, S., 2011, "An XYZ Parallel Kinematic Flexure Mechanism with Geometrically Decoupled Degrees of Freedom", *Proceedings of the ASME 2011 International Design Engineering Technical Conferences & Computers and Information in Engineering Conference*, August 29-31, 2011, Washington, DC, USA. DETC2011- 47713

14. Yun, Y., Li, Y., 2011, "Optimal Design of a 3PUPU Parallel Robot with Compliant Hinges for Micromanipulation in a Cubic Workspace", R*obotics and Computer-Integrated Manufacturing*, Vol. 27(6):977–985.

15. Hao, G., and Kong, X., 2012, "Design and Modelling of a Large-Range Modular XYZ Compliant Parallel Manipulators Using Identical Spatial Modules", *Journal of Mechanisms and Robotics*, Vol. 4: 021009.

16. http://www.thorlabs.com/navigation.cfm?guide_id=142 (Accessed on 10 February 2014)

17. http://www.physikinstrumente.com/en/products/prdetail.php?sortnr=201700 (Accessed on 10 February 2014)

18. Hao, G., Kong, X., and Reuben, R.L., 2011, "A Nonlinear Analysis of Spatial Compliant Parallel Modules: Multi-beam Modules", *Mechanism and Machine Theory*, Vol. 46(5):680–706

19. Kong, X., and Gosselin, C.M., 2007, *Type Synthesis of Parallel Mechanisms*, Springer, Berlin.

20. Hao, G., 2013, "A 2-legged XY parallel flexure motion stage with minimized parasitic rotation", *Proceedings of the IMechE, Part C: Journal of Mechanical Engineering Science*. (In press).

21. Howell, L.L., Maglegy, S.P., and Olsen B.M., 2013, *Handbook of Compliant Mechanism*s, Wiley, New York.

22. Hao, G., Meng, Q., and Li, Y., 2013, "Design of Large-range XY Compliant Parallel Manipulators Based on Parasitic Motion Compensation", *Proceedings of the ASME 2013 International Design Engineering Technical Conferences & Computers and Information in Engineering Conference*, 2013 August 4-7, Portland, Oregon, USA. DETC2013-12206

Appendix A: XYZ CPMs without overlapping SCs

A decoupled 3-DOF translational CPM with the traditional arrangement analogous to the Delta robot is shown in Fig. A.1, where the SCs associated with the three passive compliant PPRR joints do not overlap at the same point. Each leg herein can be monolithically fabricated.
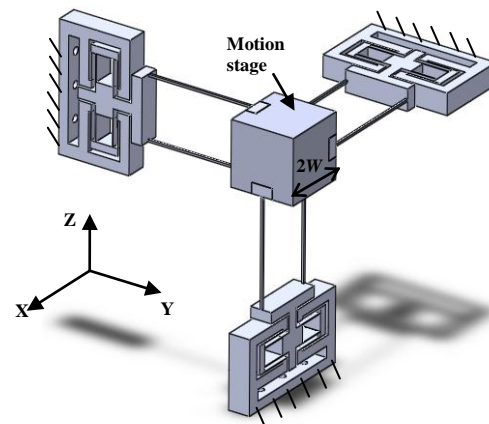

Fig. A.1 3-PPPRR XYZ CPM without overlapping SCs

In order to make the configuration more compact, two types of improved 3-PPPRR XYZ CPMs without overlapping SCs (Fig. A.2) are obtained via embedding the actuated P joint into the passive PPRR joint in each leg at the cost of sacrificing the monolithic fabrication of each leg. Alternatively, a compliant *double* two-beam module can be used as the passive compliant PPRR module for the presented two designs in Fig. A.2.
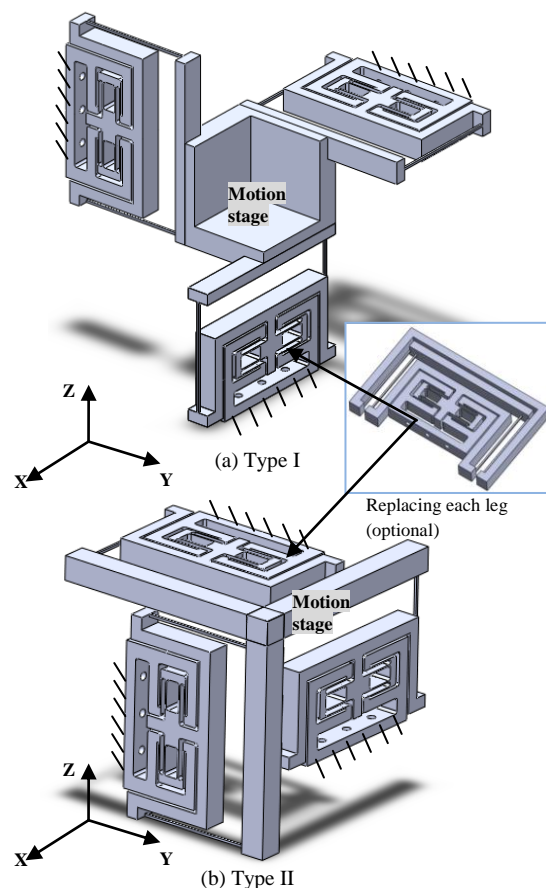

(a) Type I

(b) Type II

Fig. A.2 Compact 3-PPPRR XYZ CPMs without overlapping SCs